A sessile drop approach for studying 4H-SiC/liquid silicon high-temperature interface reconstructions

Xinming Xing, Takeshi Yoshikawa, Olga Budenkova, Didier Chaussende

A sessile drop approach for studying 4H-SiC / liquid silicon high-temperature interface reconstructions

Xinming Xing [1], Takeshi Yoshikawa [2], Olga Budenkova [1], Didier Chaussende [1] *

[1] Univ. Grenoble Alpes, CNRS, Grenoble INP (Institute of Engineering), SIMaP, F-38000 Grenoble, France

[2] Institute of Industrial Science, The University of Tokyo, 4-6-1 Komaba, Meguro-ku, Tokyo 153-8505, Japan

* corresponding author: Tel : +33 476825258 ; Email : didier.chaussende@grenoble-inp.fr

Abstract

Accurate description, understanding and control of the high temperature interface behavior between the SiC single crystal and liquid phase is critical for further development of SiC solution growth. The different parameters which create morphological instabilities, such as step bunching, micro-faceting and solvent trapping, remain unclear because they are very difficult to address in high temperature experiments. We combined experiments and numerical simulation to design a specific sessile drop approach where the liquid is removed before cooling down. The advantage of this method that it activates or suppresses the solute (carbon) transport by an AC magnetic field and thus separates the physical-chemical and hydrodynamic contributions. The method was demonstrated through observation of the morphological evolution of a 4°off 4H-SiC (0001) surface in contact with pure liquid silicon at 1600 °C according to the time factor. Several parasitic effects were also analyzed and suppressed in order to obtain a well-controlled uniform interface.

Keywords : Silicon Carbide, solid/liquid, crystal growth, reconstruction, sessile drop

1. Introduction

Silicon carbide (SiC) is an advanced functional ceramic offering a unique combination of chemical, physical and mechanical properties. It is also a wide bandgap semiconductor which is currently bringing about an in-depth change to power electronics because it significantly improves the efficiency of electric energy conversion and distribution [1, 2]. Today, high quality 6-inch diameter 4H-SiC single crystalline wafers are available. These wafers are all produced by a seeded sublimation

technique, often referred to as physical vapor transport (PVT) method [3]. Over the past decade, the top seeded solution growth (TSSG) method has been studied with the aim of obtaining ultimate quality 4H-SiC wafers. If TSSG is carried out at lower temperatures and with lower temperature gradients than for the PVT process, it is inherently more suitable for reducing residual stress and associated defect density [4]. Furthermore, TSSG has been observed to have a very efficient dislocation conversion mechanism based on the interaction between the dislocation lines and the steps moving along the crystal growth front [5, 6]. Whether the surface is nominal or vicinal, growth occurs through the movement of steps at the crystal surface associated with one or a combination of mechanisms, namely the layer-by-layer, step flow and spiral growth mechanisms [7]. However, the formation of macro-steps by step-bunching, and the occurrence of micro-faceting give rise to macroscopic surface roughening, the formation of trenches and the inclusion of solvent which all severely degrade the quality of the crystal [8, 9]. Understanding and controlling the behavior of steps during SiC solution growth are still critical to obtain a stable growth front.

Several approaches have been suggested to reduce step bunching such as the addition of metallic elements into molten silicon [10, 11] or the use of seeds with different orientations and azimuth angles [12]. Yet the behavior of the steps at the Liquid-SiC interface remains unclear because of the complexity of the growth environment, i.e. the strongly coupled energetic, kinetic or hydrodynamic phenomena which influence the steps. *In situ* observation research also provided some fundamental data on the step behavior [13, 14] but the conditions applied to the interface in this kind of small observation device meant isolating the different contributing parameters was not possible. In fact, work on the description of the surface reconstruction of 4H-SiC single crystal in contact with the high temperature solution is still in progress.

We developed a methodology that ensures a reproducible and accurate *ex situ* observation of the liquid/solid interface. The experimental concept is based on the sessile drop method and makes it possible to apply a well-controlled environment to the interface. The interface structure between 4H-SiC and liquid silicon and the morphological evolution associated to dissolution of the SiC can be demonstrated as an illustration of this method. This approach can be extended to many other ceramics/solvent systems.

2. Experimental

This experiment consists of making a silicon droplet react on a SiC single crystalline substrate in a well-controlled environment. After a given time and at a given temperature, the liquid is removed at a high temperature to “freeze” interfacial reconstruction and avoid any further evolution. The SiC surface is then examined ex-situ.

The experimental apparatus is a laboratory scale, high temperature induction furnace as shown in Figure 1. The chamber consisted of a vertical water-cooled quartz jacket. It was closed by two stainless steel flanges, fitted with openings for measurements, observations and sample handling. The

external induction coil was fixed on a vertical translation to change its relative position with respect to the crucible. This meant the temperature distribution inside the crucible could be adjusted, especially the axial temperature gradient. The heating zone was composed of high density, high purity graphite parts insulated with rigid graphite felt. The external graphite part acted as a susceptor for direct induction heating which is mainly performed at medium frequency and was at 22 kHz in these experiments. The inner part of the heating zone was mainly heated by the thermal radiation emitted by the susceptor. The samples consisted of SiC substrate with a silicon piece on top and were placed on a flat graphite holder, located approximately in the center of the heating zone. Some experiments were performed with a Ta tube placed around the sample to shield it from the electromagnetic field. The temperature was measured both from the top (on the sample holder) and the bottom (at the back side of the sample holder, very close to the SiC substrate) using bi-chromatic optical pyrometers which were periodically calibrated with a set of fixed points. The heating power was adjusted according to the bottom temperature measurement. A tool which was slightly inclined with respect to the symmetry axis was used to remove the liquid from the SiC substrate at high temperature, i.e. before cooling down. It consisted of a graphite rod, terminated by a Tantalum sheet. The high affinity of liquid Si with the high melting point metals such as W, Nb, and Ta means that liquid silicon wets the tantalum sheet very well and very quickly. The whole liquid silicon droplet could thus be removed in less than one second by wetting the Ta sheet.

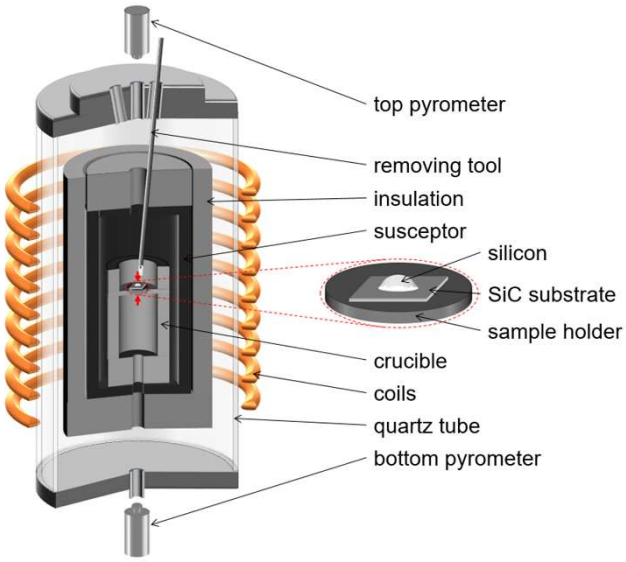

Figure 1 Schematic drawing of the experimental apparatus used for the interface reconstruction experiments. The heating zone (external surfaces of the graphite insulations) was 300 mm high with a diameter of 130 mm. Red arrows indicate the locations of the temperature measurements.

A 2 mm-thick electronic grade silicon wafer was used as the silicon source. Small squares of 2.0*2.0 mm² were cut using a high precision dicing saw, ensuring a precise and reproducible amount of silicon. The SiC pieces came from commercial 4H-SiC substrates with a miscut angle of 4° towards

the <11-20> direction. The Si-terminated surface was chemical mechanically polished (CMP) to ensure a surface free of subsurface damage. After degreasing in acetone followed by ethanol using an ultrasonic bath, both the Si piece and the SiC substrate were deoxidized in dilute HF solution for 10 mins, rinsed by deionized water for 1 min and then transferred onto the graphite sample holder in the crucible. The chamber was firstly vacuumed during the heating stage to outgas the crucible and then filled with Argon (6N, up to 950 mbar) at high temperature. Then, the crucible was heated up to the required temperature at a rate of 20 °C/min. During the heating phase, the Si piece melted on the SiC substrate forming a droplet. The experiments were kept for various times and temperatures. At the end of the experiments, the liquid droplet was quickly absorbed before cooling down. This ensured the real high temperature interface structure was conserved for further ex-situ characterizations, by preventing any crystallization of SiC from the saturated liquid droplet during cooling down. The SiC sample was then dipped in a HF: HNO_3 aqueous solution to remove the Si residues. After rinsing and blowing, the surface morphology was systematically observed using an optical microscope in the Nomarski differential interference contrast (NDIC) mode. The global 3D topography of the liquid Si/SiC interface was scanned with a mechanical profilometer (Talysurf 50, Taylor Hobson) and areas of interest were probed using an atomic force microscope (AFM) in tapping mode (Dimension 3100, Digital instruments).

Numerical simulations were carried out using the finite element method (FEM) with the COMSOL Multiphysics^{TM} software package. A stationary study was carried out with a two-dimensional axisymmetric model to replicate the geometry of the real reactor including the induction coil and with a droplet of fixed shape. The electromagnetic problem was solved in the frequency domain and coupled with the calculation of the temperature distribution in the system. Based on the latter, the density of AC current circulating in the coil was adjusted to meet a temperature of 1600 °C at the SiC/liquid interface. Furthermore, effective electromagnetic force acting in the drop was introduced in the Navier-Stokes equation. The Si melt was considered to be an incompressible Newtonian fluid and the fluid flow generated by the Lorentz force was assumed to be laminar. We did not consider buoyancy convection related to the solutal gradient because the carbon solubility was very small, typically less than 0.1 at% within the temperature range under study [15]. Details of such numerical calculations can be found elsewhere [16, 17].

3. Results and discussion

3.1. Thermal design

The relative position between the crucible and the coil was chosen by means of numerical simulation to obtain minimum temperature gradients in and around the liquid droplet (Figure 2). The temperature in the central part of crucible was homogeneous, with typical temperature gradients being 1 °C.cm^{-1}, along 5 cm from the droplet center, both in radial and axial directions (Figure 2a). The samples were subjected to very low temperature gradients because of the small size of the droplet (typically 4 to 5

mm in diameter) as compared to the large homogeneous hot zone. This is illustrated by the close-up on the droplet shown in Figure 2b, where the temperature variation inside the droplet, and particularly along the liquid-solid interface, was found to be less than 0.1 °C at a sample temperature of 1600 °C.

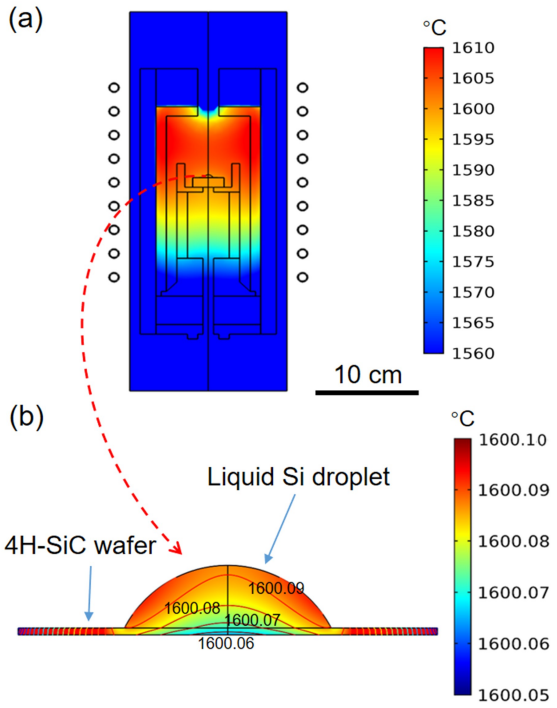

Figure 2 a) computed temperature distribution in the crucible; b) focus on the temperature distribution in the droplet. Temperature isoline step: 0.01 °C.

3.2. Formation of the liquid-solid interface

To limit vaporization of liquid silicon at high temperature, all the experiments were carried out under argon pressure close to the atmospheric one (>900 mbar). For practical reasons, the temperature was kept constant while filling the chamber with Ar, which explains the presence of a temperature plateau of a few minutes during Ar injection. Figure 3 shows two different temperature/argon injection profiles, the first (a) with Ar filling at 1100 °C and the second (b) with Ar filling at 1450 °C, i.e. respectively before and after the melting of Si. The NDIC images of the substrate surface obtained in these experiments are shown in the insets to the graphs. The temperature at which Ar was injected in the reactor had a very strong effect on the interface morphology, as will be discussed hereafter.

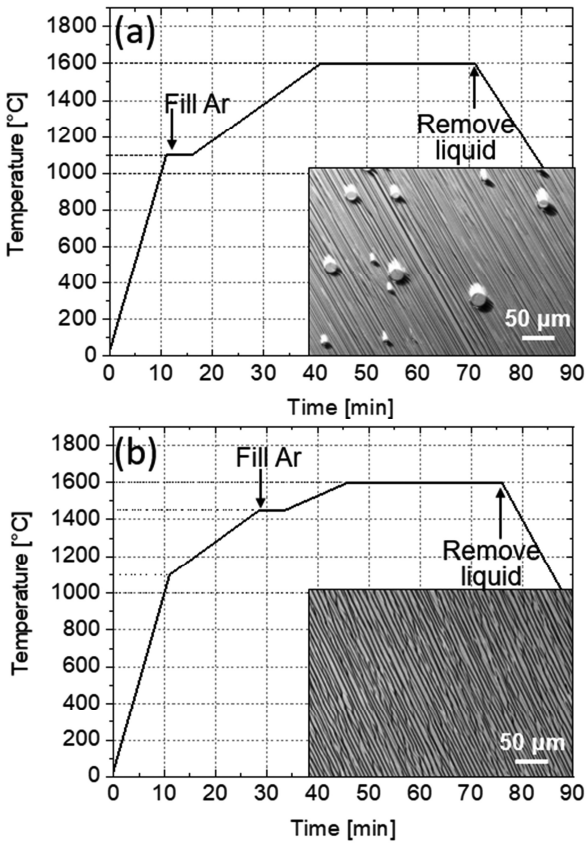

Figure 3 two different temperature profiles for 4H-SiC, 4°off Si-face surfaces treated at 1600 °C for 30 minutes. The main difference is the temperature at which the reactor is filled with Ar: a) at 1100 °C, b) at 1450 °C (just after Si melting). The insets are the corresponding surface morphologies observed using NDIC optical microscopy.

As liquid silicon is a solvent for SiC, and despite the very limited solubility of the latter, the first stage of the formation of the liquid-solid interface is the dissolution of the top surface of SiC. The initial SiC surface obtained right after CMP polishing is composed of steps with typically one Si-C bilayer height (0.25 nm) [18]. During the dissolution process, these bilayer steps bunched together forming ordered step-terrace arrays with larger terraces and higher steps. This dominant feature was observed on both NDIC pictures of Figure 3, where the Si-terminated 4°off 4H-SiC surfaces were in contact with liquid silicon at 1600 °C for 30 minutes. Also many circular prints were observed, randomly scattered on the SiC surface (Figure 3a) when the argon was injected at 1100 °C during the heating stage. However, these features did not appear when the argon was injected at 1450 °C, i.e. just after the melting of silicon (Figure 3b). An AFM picture of one of the circular prints is shown in Figure 4a. The height profile along the white line was plotted in Figure 4b. The circular hillock was characterized by a flat top surface, with an appearance similar to the pristine surface. All around, the surface evolved significantly, generating a train of steps with width in the micrometer range. The hillock thus appeared as a discontinuity of the interface morphological evolution. In addition, the height difference between the top of the hillock and the average altitude of the surrounding was

measured at about 220 nm. For comparison, an assessment of the thickness of SiC dissolved during equilibration of SiC and the liquid Si droplet was carried out (see Figure ESM-1 in supplementary material). Based on the solubility dataset from Scace et al.[15], the computed dissolved depth was found to be of around 143 nm at 1600 °C, within the same range as the measured height of the hillock. We thus concluded that these hillocks corresponded to undissolved areas, or, in other words, areas where the liquid silicon was not in contact with SiC, most probably because of the presence of bubbles trapped at the liquid/SiC interface.

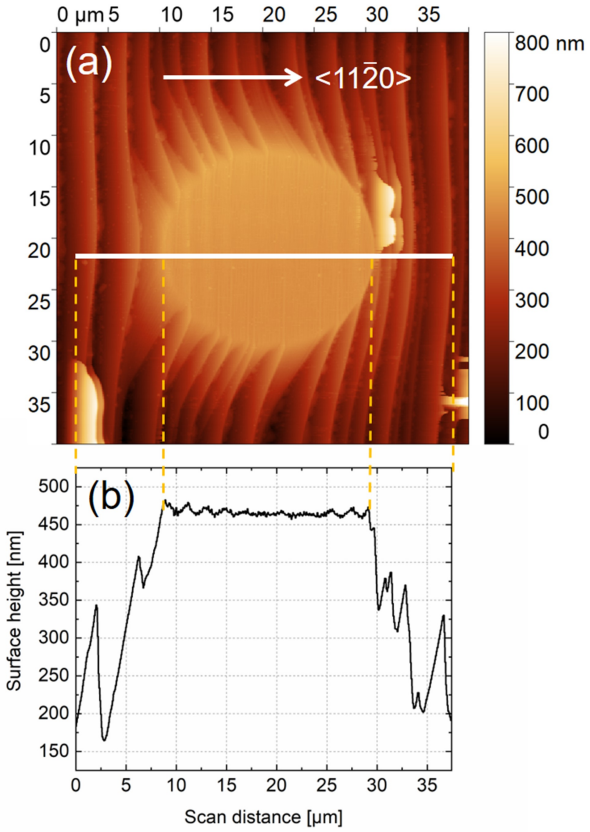

Figure 4 a) AFM picture showing the effect of a bubble trapped at the liquid/solid interface upon melting. b) Height profile along the hillock. This sample corresponds to a Si-face treated at 1600 °C for 30 minutes. The <11$\bar{2}$0> direction is indicated in a).

A first scenario for explaining these hillocks was that these were caused by the generation of SiO(g) at the interface, due to the reaction between the Si and the native SiO_2 layer on the SiC substrate [19] :

$$Si(l)+SiO_2(s)\rightarrow 2SiO(g) \qquad (1)$$

At room temperature, a thin oxide layer of few nanometers is usually formed on the surface of SiC wafer [20]. Even if the oxide layer was still partially present at the interface before the melting of Silicon, a complete conversion into SiO(g) could not explain the amount of circular prints observed. In addition, previous works showed that in Ar of commercial purity (lower in purity than the Ar we

used), there is no longer an oxide layer at the SiC surface at temperatures T>1100 °C due to active oxidation [21]. Thus, at the Si melting point, both Si and SiC are deoxidized which means a gapless liquid/solid contact should be formed instantaneously, thus ruling out this first scenario.

A second scenario was suggested by the experimental result shown in Figure 3 and involved the entrapment of argon at the interface during melting. Mitani et al. demonstrated that during TSSG of SiC, the formation of voids in the grown crystal could be attributed to the entrapment of Ar bubbles at the growth front [22]. To explain this, they speculated that Ar, initially dissolved in the solvent, vaporized and formed bubbles during the crystal growth process. In our case the effect was similar but the origin of the bubbles was different. If the bubbles had come from dissolved argon, we would have observed hillocks along the whole liquid/SiC interface and yet hillocks were only found where the solid Si piece was originally located, before melting (see figure ESM-2). This suggests that the argon was already present between the two solid pieces and then entrapped at the interface upon melting. Therefore, by melting the silicon under a vacuum and filling the Argon at 1450°C - i.e. once the liquid/solid interface was formed - no more hillocks were observed at the surface.

3.3. The effect of electromagnetic mixing

There was a dual aim to using the AC electromagnetic field (EMF) in the experiment. Firstly, it allowed inductive heating of the susceptor. Secondly, at a certain AC frequency, the EMF can be used to generate forced convective flow in the droplet. These effects are discussed in detail in this section.

When an alternative magnetic field penetrates an electric conductor, its magnitude decreases exponentially owing to the energy loss. The penetration depth (δ) defines the distance at which the magnetic field has been attenuated to 1/e of its magnitude at the conductor's surface [23]. The value of δ is expressed as:

$$\delta = \sqrt{\frac{2}{\omega\mu\sigma_{el}}} = \sqrt{\frac{1}{\pi f \mu_r \mu_0 \sigma_{el}}} \quad (2)$$

where f is the frequency of the EMF (or alimenting electric current AC) (Hz), μ_r is the relative permeability of the material (usually =1 for conductors), μ_0 is the permeability of the vacuum (= $4\pi \times 10^{-7}$ H.m^{-1}) and σ_{el} is the electrical conductivity of the material. The electrical conductivity of Tantalum and graphite as a function of temperature are given in equations (3) and (4) respectively, expressed in S.m^{-1}. For Ta, this was obtained from the data reported by Desai et al. [24]. For graphite, it is the optimized polynomial form, used for numerical simulation of SiC sublimation growth process [25].

$$\sigma_{Ta}(T) = 2.3923 \cdot 10^7 \cdot e^{\left(\frac{-T}{116}\right)} + 7.1739 \cdot 10^6 \cdot e^{\left(\frac{-T}{338}\right)} + 2.6234 \cdot 10^6 \cdot e^{\left(\frac{-T}{1572}\right)} + 4.9657 \cdot 10^5 \quad (3)$$

$$\sigma_C(T) = -6.519 \cdot 10^{-9} \cdot T^4 + 6.091 \cdot 10^5 \cdot T^3 - 1.915 \cdot 10^{-1} \cdot T^2 + 2.242 \cdot 10^2 \cdot T + 3.247 \cdot 10^4 \quad (4)$$

The dependence of the penetration depth on temperature in graphite and Ta was calculated for different AC frequencies (Figure 5). For f=22 kHz, at 1600°C (1873 K), the penetration depth was 10.5 mm in graphite, which is thicker than our graphite susceptor. That means that at this AC frequency a fraction of EMF propagates through the crucible and may affect the electrically conducting sample (the droplet). A shield made of Ta can be introduced into the furnace to avoid the EM field having a direct effect on a drop. Computation of the power volumetric loss density in the crucible, both with and without the Ta shield (Figure ESM-3) showed that the Ta tube dissipated a large part of the EMF through Joule losses, significantly reducing the magnetic field density applied on the droplet. Our experiments were performed using these configurations. Alternatively, the direct effect of the electromagnetic field on the droplet can be reduced by increasing the AC frequency which makes the penetration depth of the magnetic field smaller according to eq.2. For instance, at 280 kHz, the penetration depth in graphite was reduced to 3 mm which is thus much smaller than the thickness of the susceptor.

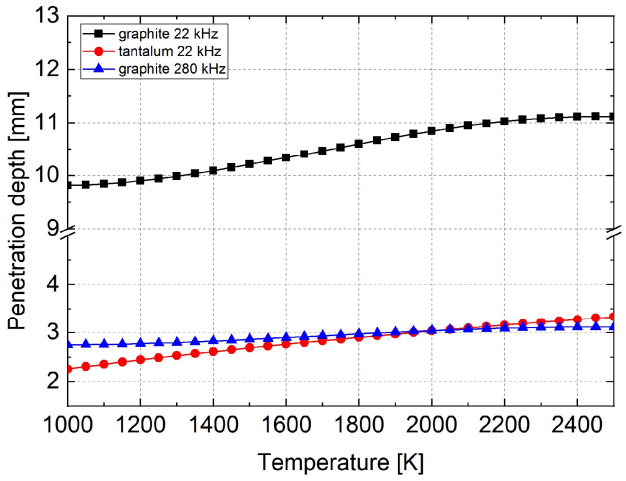

Figure 5 Penetration depth as a function of temperature in graphite and tantalum calculated from equation 2. For graphite, two different frequencies were considered for the calculation.

Interestingly, the effect of the electromagnetic field on the droplet can be revealed through characterization of the liquid/ SiC interface. To demonstrate this, the whole liquid/SiC interface topography was characterized by a mechanical profilometer, for two different experiments: in the first, the configuration is as shown in Figure 1, and in the second with the sample and graphite holder placed in a 1 mm-thick Ta tube (Figure 6).

- In the experiment performed without Ta tube, the interface was concave, with the edge of the droplet at a higher level than the central area, and even higher than the initial SiC surface. This implies that mass transport could occur, from the center to the edge of the droplet.
- In the experiment performed with the Ta tube, the interface was almost flat, though slightly

below the initial surface level due to the SiC dissolution.

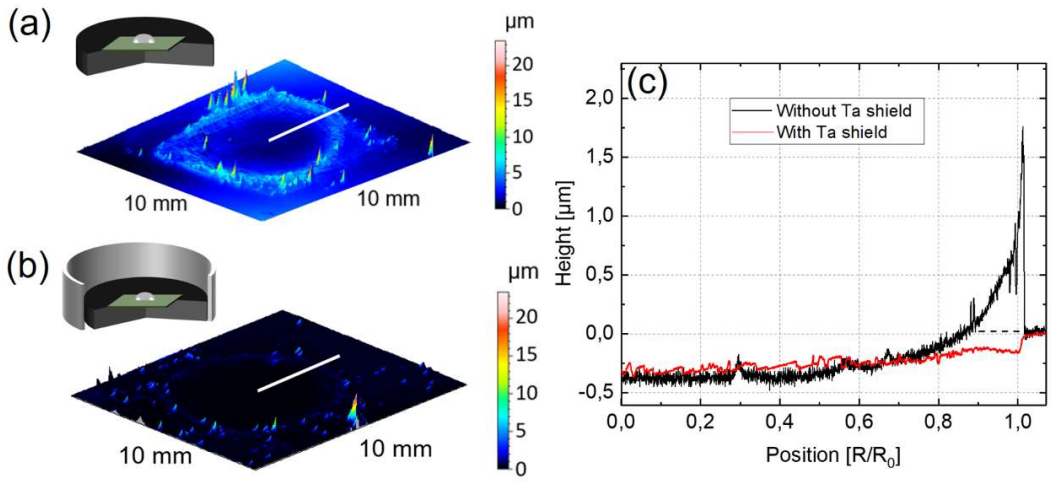

Figure 6 3D topography of the whole liquid/solid interaction area, mapped with a mechanical profilometer. These two samples were treated using the same conditions (1600 °C, 30 min) except: a) without Ta shield; b) with a Ta shield. c) Plot of the measured height profile along the radius of the liquid-solid interface shown as white line in a) and b).

In electrically conductive liquids subjected to monophase AC electromagnetic field, the motion of the liquid can come from the action of Lorentz forces. Their action takes place inside the liquid Si droplet near its surface and generates liquid motion along the droplet basis from its edge to the center which is compensated by the downward flow along the droplet free surface (see Figure ESM-4). The calculations were performed with the fixed shape of the droplet assuming a no-slip condition at the SiC/liquid interface and the absence of shear on the droplet free surface. The use of the Ta shield does not change the character of the flow, i.e. the shape of the convective vortex. However, its presence makes the intensity of the fluid velocity (size of the velocity vectors) significantly weaker. Again, this has to be linked with the shielding effect of the Ta tube with respect to the electromagnetic field.

3.4. Discussion:

High temperature experiments are always very challenging, especially when the aim is to uncouple the complex mixture of phenomena. A quasi-isothermal condition, achieved through the proposed sessile drop method, is the requirement for observing the formation of the “native structure” of the solid-liquid interface. This ensured that after the initial, transient dissolution of the SiC surface, there was no more temperature driven evolution of the SiC/liquid interface. Then, once the liquid was thermodynamically equilibrated with SiC, the activity of carbon in the liquid becomes uniform. All the carbon transport phenomena related to the temperature gradient can be ruled out. This is the case for i) Fick’s diffusion as the carbon activity is uniform, ii) natural convection as the liquid density is

uniform, iii) Marangoni convection, as the surface tension of the liquid is uniform. This is very important for the latter contribution as Marangoni convection can be activated by a very small temperature gradient along a free liquid silicon surface, of about 2 °C.cm^{-1} [16].

Electromagnetic forces thus remain the only actuator that can be used to activate or suppress carbon transport in the droplet. Figure 7 summarizes our sessile drop approach, by describing the evolution of the dissolved thickness at the droplet center as a function of time, t_0 corresponds to melting of silicon, taken here as the starting time. This diagram has to be correlated with Figure 8, where the surface morphology and step statistics are displayed for the different cases, taken beyond t_1. Here the substrates were treated at 1600 °C for different times, with and without the Ta tube. All the pictures were taken using NDIC microscopy at the center of the wetting area. The corresponding distributions of step spacing were obtained by picture processing, using the ImageJ^{TM} software.

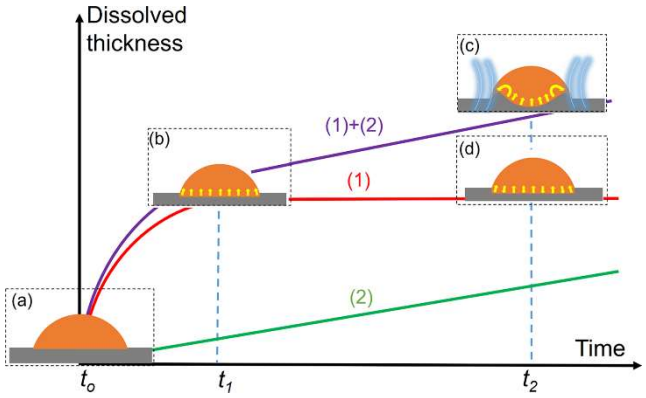

Figure 7 schematic drawing of the dissolved thickness at the droplet center as a function of time. (1) chemical contribution, (2) transport contribution due to electromagnetic field, (1) + (2) sum of both. t_1-t_0 is the time needed to saturate the liquid while t_2-t_0 denotes the total reconstruction time before removing the liquid, indicated states a,b,c and d are discussed in the text.

Initially, the pure Si melt was not in thermodynamic equilibrium with SiC (Figure 7a). The first step, from t_0 to t_1, thus consists in the dissolution of the SiC wafer to saturate the Si droplet with carbon (Figure 7b). Once the system is equilibrated at t_1 , a dynamic dissolution/precipitation equilibrium takes place at the interface. There will be apparently no further evolution of the system (curve (1)). This is the case when the Ta tube is used, screening the electromagnetic field and thus reducing the carbon transport issued from electromagnetic convection. The shape of the interface remains flat (Figure 6b and 7d), and the surface morphology does not exhibit major evolution between 30 mins and 240 mins (Figure 8c,d), a result which is also supported by the statistical treatment of the step spacing (Figure 8f). It should be noted that this kind of wavy morphology was already obtained after 5 mins at 1600 °C (see Figure ESM-5), suggesting that the initial dissolution stage (t_1) is rather fast, taking less than a few minutes.

The contribution of the EM convection is depicted with curve (2) in Figure 7. We assume that it corresponds to a stationary transport of carbon from the center to the edge, giving rise to a constant, slow dissolution rate at the center (slope of the curve). The actual interfacial reconstruction process without the Ta tube is thus the sum of curves (1) and (2). After the fast initial dissolution, a stationary dissolution state applies at the center of the droplet area. The interface slowly becomes concave due to the carbon transport from the center to the edge. In this case, the surface morphology is rather different and evolves with time. Between 30 mins and 180 mins, the steps were progressively bunched up, as evidenced by the step spacing statistics (Figure 8a,b,e). Assuming that Figures 8c,d (without C transport) correspond to a stabilized morphology, Figures 8a, b can be associated to morphological evolution at certain degree of undersaturation close to the interface and can thus be described by the standard BCF theory of crystal growth [27]. The significantly different morphologies observed whether the dissolution is transient (the initial one, without EM field) or stationary (with EM field) supports the proposed methodology, which offers the possibility to activate/deactivate the stationary transport of solute from the liquid/SiC interface.

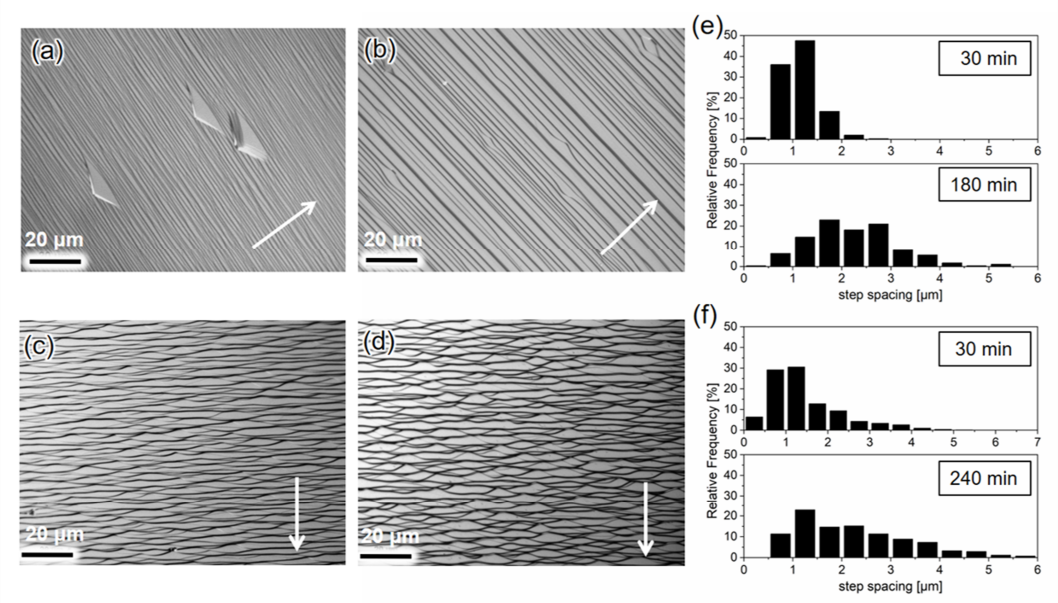

Figure 8 Surface morphologies observed by NDIC optical microscopy of 4H-SiC, 4°off Si-face surfaces treated at 1600 °C. a) for 30min, without EM shield; b) for 180min, without EM shield; c) for 30min, with EM shield and d) for 240min, with EM shield. The pictures were taken in the centre area. At the right the corresponding distribution of step spacing are displayed: e) without EM shield and f) with EM shield. The <11$\bar{2}$0> direction is marked with white arrow in all the NDIC photos.

To get rid of any parasitic effect linked with the Ta tube, like local temperature variations due to modification of radiative heat transfer, we tried to reduce the EM contribution by using a higher frequency furnace (280 KHz). This was expected to significantly reduce the penetration depth in graphite, as calculated in Figure 5. With the other conditions being identical, the surface morphology

of both samples, with Ta tube at 22 kHz and without Ta tube at 280 kHz, were found to be very similar (Figure ESM-5). This validated the idea that the Ta tube only affected the magnitude of the EM field. This further implies that EM forces worked as the main actuator for the carbon transport and consequently the morphological evolution.

Another important aspect to discuss is the behaviour of the free surface (the liquid-vapour LV interface) and especially of possible mass transfers at the LV interface. In our system, we considered that the SiC wafer is the only source of carbon, through dissolution (curve 1 in Figure 7). This supposes that there is no carbon flux crossing the LV interface. Working under reactive gases, such as CH_4 or any carbon precursor, or with species able to react with carbon like H_2 or O_2, would either supply carbon to or extract carbon from the droplet. This phenomenon has been widely used in the case of the Vapour-Liquid-Solid growth process for instance [26, 27]. However, this would imply a continuous dissolution or growth of the SiC surface, i.e. that it would add a constant slope like in curve 2 of Figure 7. This was not observed in our case for long experiments carried out with EM shielding. We can thus assume that carbon transfer through the LV interface is negligible and that the purity of the gas ambient is sufficient to suppress any interaction with the gas phase of a chemical nature. The same idea applies to silicon atoms of the solvent that can vaporize at the LV surface. This would produce two effects: i) supersaturation of the droplet due to the progressive loss of solvent, ii) cooling of the free surface due to the latent heat of vaporization. Both effects would result in SiC crystallization, but not necessarily in the same location of the droplet. At 1600 °C we could not detect any significant loss of silicon even after a long time. Nevertheless, this effect should be seriously considered at higher temperature, as the vaporization rate is expected to increase exponentially with temperature.

Finally, it is important to mention the so called ridge effect, described in works on wetting [28]. This effect would basically produce a similar shape to the one observed close to the droplet edge in figure 6a. When induced by a very local force balance at the VLS triple line which enhances the interfacial reconstruction, this is usually effective over a much smaller spatial extent that our observation. If this is present, it should not disappear when EM shielding is used. Consequently, we do not consider this to be a determining factor in our experiments.

4. Conclusions

A new method, based on a sessile drop approach, was implemented for the study of the high-temperature interface morphology between 4H-SiC and silicon solvent. An isothermal environment was designed to get rid of any contribution from temperature gradients (Marangoni convection, diffusion, etc.). An AC magnetic field was used as an actuator for carbon transport and its effect was demonstrated based on a coupled approach, using experiments and numerical simulation. Without electromagnetic forces, after the initial dissolution of the SiC surface, there is almost no evolution of the interface structures and the morphology can be considered as in an equilibrium after a few

minutes. While applying electromagnetic forces onto the liquid droplet, a stationary solute transport is generated along the interface, maintaining a constant undersaturation (dissolution) at the center of the droplet. Using the electromagnetic field thus allows switching from static to dynamic dissolution of the SiC crystal, which is ideal for studying the interface behavior, and especially the step dynamics. Additionally, the temperature at which the reactor is filled with argon was found to be a critical factor in avoiding bubbles forming at the interface. We believe that such an approach could be of great help in understanding the crystal/solvent interface behavior in SiC solution growth and could also be potentially applied to many other high temperature chemical systems.

Acknowledgements

Dr. Jean-Marc Dedulle and Dr. Yves Du Terrail Couvat are greatly acknowledged for their help on Comsol simulations. This work was supported by a French-Japanese partnership (PRC CNRS-JSPS). X. Xing acknowledges a scholarship from the China Scholarship Council (No. 201806460011).

References

1. Eddy CR, Gaskill DK (2009) Silicon carbide as a platform for power electronics. Science 324:1398–1400. https://doi.org/10.1126/science.1168704
2. Kimoto T, Cooper JA (2014) Fundamentals of Silicon Carbide Technology: Growth, Characterization, Devices and Applications. John Wiley & Sons Singapore Pte. Ltd
3. Chaussende D, Ohtani N (2019) 5 - Silicon carbide. In: Fornari R (ed) Single Crystals of Electronic Materials. Woodhead Publishing, pp 129–179
4. Hofmann DH, Muller MH (1999) Prospects of the use of liquid phase techniques for the growth of bulk silicon carbide crystals. Mater Sci Eng B-Solid State Mater Adv Technol 61–2:29–39. https://doi.org/10.1016/s0921-5107(98)00440-1
5. Harada S, Yamamoto Y, Seki K, et al (2013) Evolution of threading screw dislocation conversion during solution growth of 4H-SiC. Apl Mater 1:022109. https://doi.org/10.1063/1.4818357
6. Harada S, Yamamoto Y, Seki K, et al (2014) Different behavior of threading edge dislocation conversion during the solution growth of 4H-SiC depending on the Burgers vector. Acta Mater 81:284–290. https://doi.org/10.1016/j.actamat.2014.08.027
7. Markov IV (2003) Crystal growth for beginners: fundamentals of nucleation, crystal growth and epitaxy. World scientific
8. Kamei K, Kusunoki K, Yashiro N, et al (2009) Solution growth of single crystalline 6H, 4H-SiC using Si–Ti–C melt. J Cryst Growth 311:855–858. https://doi.org/10.1016/j.jcrysgro.2008.09.142
9. Zhu C, Harada S, Seki K, et al (2013) Influence of Solution Flow on Step Bunching in Solution Growth of SiC Crystals. Cryst Growth Des 13:3691–3696. https://doi.org/10.1021/cg400706u

10. Komatsu N, Mitani T, Hayashi Y, et al (2017) Modification of the surface morphology of 4H-SiC by addition of Sn and Al in solution growth with SiCr solvents. J Cryst Growth 458:37–43. https://doi.org/10.1016/j.jcrysgro.2016.10.045
11. Mitani T, Komatsu N, Takahashi T, et al (2015) Effect of aluminum addition on the surface step morphology of 4H-SiC grown from Si-Cr-C solution. J Cryst Growth 423:45–49. https://doi.org/10.1016/j.jcrysgro.2015.04.032
12. Mitani T, Komatsu N, Hayashi Y, et al (2017) Morphological stability of 4H-SiC crystals in solution growth on {0001} and {1$\bar{1}\bar{0}$m} surfaces. J Cryst Growth 468:883–888. https://doi.org/10.1016/j.jcrysgro.2016.12.107
13. Kawanishi S, Yoshikawa T, Morita K, et al (2013) Real-time observation of the interface between SiC and a liquid alloy and its application to the dissolution behavior of SiC at 1573 K. J Appl Phys 114:1.4837575. https://doi.org/10.1063/1.4837575
14. Onuma A, Maruyama S, Komatsu N, et al (2017) Quantitative Analysis of Nanoscale Step Dynamics in High-Temperature Solution-Grown Single Crystal 4H-SiC via in Situ Confocal Laser Scanning Microscope. Cryst Growth Des 17:2844–2851. https://doi.org/10.1021/acs.cgd.7b00325
15. Scace RI, Slack GA (1959) Solubility of Carbon in Silicon and Germanium. J Chem Phys 30:1551–1555. https://doi.org/doi:http://dx.doi.org/10.1063/1.1730236
16. Mercier F, Dedulle JM, Chaussende D, Pons M (2010) Coupled heat transfer and fluid dynamics modeling of high-temperature SiC solution growth. J Cryst Growth 312:155–163. https://doi.org/10.1016/j.jcrysgro.2009.10.007
17. Lefebure J, Dedulle JM, Ouisse T, Chaussende D (2012) Growth rate prediction in SiC solution growth using silicon as solvent. pp 69–72
18. Vicente P, Pernot E, Chaussende D, Camassel J (2002) Atomic-step observations on 6H- And 15R-SiC polished surfaces. pp 729–732
19. Brewer L, Edwards RK (1954) The stability of SiO solid and gas. J Phys Chem 58:351–358
20. C. Önneby, C. G. Pantano (1997) Silicon oxycarbide formation on SiC surfaces and at the SiC/SiO2 interface. J Vac Sci Technol A 15:1597–1602. https://doi.org/10.1116/1.580951
21. Jacobson NS (1993) Corrosion of Silicon-Based Ceramics in Combustion Environments. J Am Ceram Soc 76:3–28. https://doi.org/10.1111/j.1151-2916.1993.tb03684.x
22. Mitani T, Okamura M, Takahashi T, et al (2012) Control of void formation in 4H-SiC solution growth. pp 57–60
23. Jordan EC, Balmain KG (1968) Electromagnetic waves and radiating systems. Prentice-Hall
24. Desai PD, Chu TK, James HM, Ho CY (1984) Electrical resistivity of selected elements. J Phys Chem Ref Data 13:1069–1096. https://doi.org/10.1063/1.555723
25. Ariyawong K (2015) Process modeling for the growth of SiC using PVT and TSSG methods. Université Grenoble Alpes

26. Chaussende D, Ferro G, Monteil Y (2002) Vapour-liquid-solid mechanism for the growth of SiC homoepitaxial layers by VPE. J Cryst Growth 234:63–69. https://doi.org/10.1016/S0022-0248(01)01651-7
27. Ferro G, Chaussende D, Jacquier C (2006) VLS growth of SiC epilayers. In: Syväjärvi M, Yakimova R (eds) Wide Band Gap Materials and New Developments. Research Signpost, Kerala, INDIA, pp 91–116
28. Saiz E, Tomsia AP, Cannon RM (1998) Ridging effects on wetting and spreading of liquids on solids. Acta Mater 46:2349–2361. https://doi.org/10.1016/S1359-6454(98)80016-5

SUPPLEMENTARY MATERIAL

A sessile drop approach for studying 4H-SiC / liquid silicon high-temperature interface reconstructions

Xinming Xing, Takeshi Yoshikawa, Olga Budenkova, Didier Chaussende *

* corresponding author: Tel : +33 476825258 ; Email : didier.chaussende@grenoble-inp.fr

ESM-1. Calculation of the dissolved SiC thickness

The computed dissolved depth was based on the solubility dataset from Scace et al. [1]. A value of about 143 nm was found at 1600 °C, within the same range as the measured height of the hillock. The calculated value was slightly smaller, but the solubility curve is still controversial to date. The data from Scace et al. have the benefit of having been measured along the widest temperature range reported. They are also considered by some authors as underestimating the solubility. Accordingly, we think that both the calculated and the experimental values were in agreement.

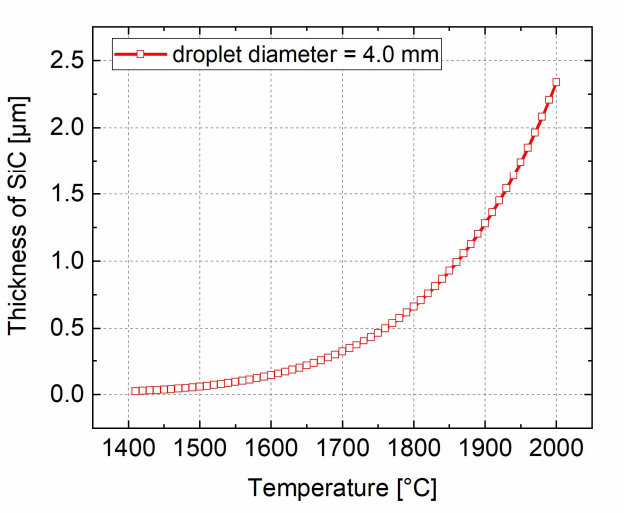

Figure ESM-1 calculated thickness of SiC dissolved as a function of temperature, for a droplet diameter of 4.0 mm at equilibrium.

ESM-2. Illustration of the location of the hillocks

After melting, the hillocks were only observed at the initial interface between the solid Si piece and the SiC substrate. Thus, the hillocks are all inscribed in a square, which corresponds to the face of the Si cube initially in contact with the SiC substrate.

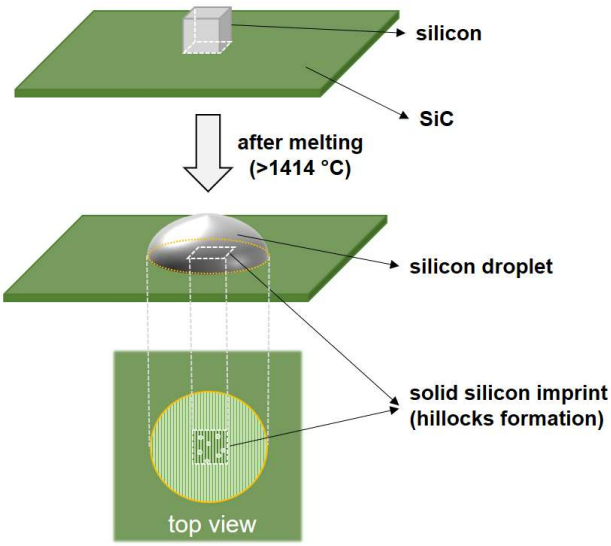

Figure ESM-2 Schematic drawing illustrating the location of the hillocks, formed at the Si/SiC interface.

ESM-3. Computation of the power volumetric loss density in the crucible

Computation of the power volumetric loss density in the crucible, both with and without the Ta shield. The other parts were made of graphite. The Ta tube dissipated a large part of the electromagnetic field through Joule losses, reducing significantly the magnetic field density applied on the droplet. It thus acted as an electromagnetic shield.

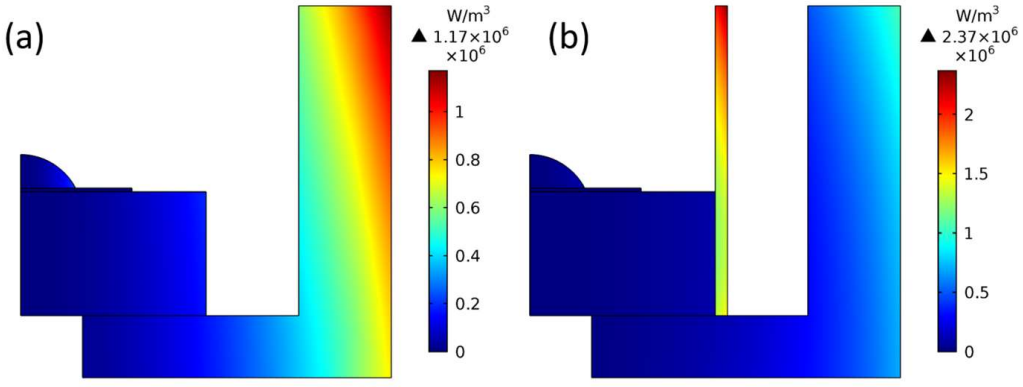

Figure ESM-3 computed volumetric loss density into and around the sample a) without and b) with the Ta tube (shield). Representations are given for half of the inner part of the crucible as it is considered as axi-symmetrical.

ESM-4. Computation of the electromagnetic convection contribution

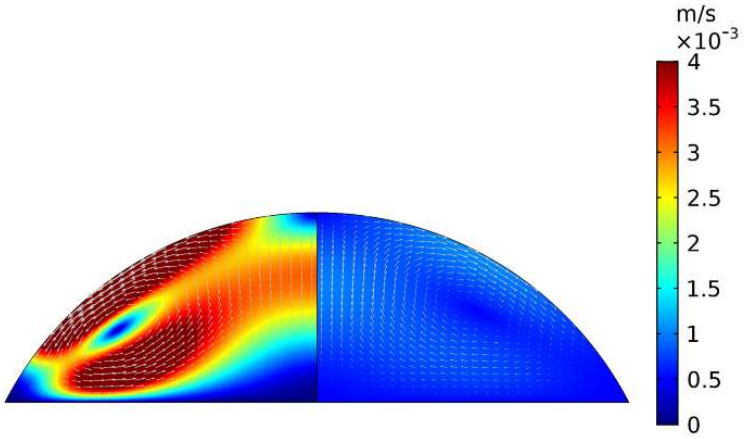

Figure ESM-4 Mass transport as computed in the droplet. The white arrows correspond to magnitude of the fluid velocity. Left) without EM shielding and right) with an EM shielding (Tantalum tube); Note here that only a half droplet is presented.

ESM-5. Short time morphology

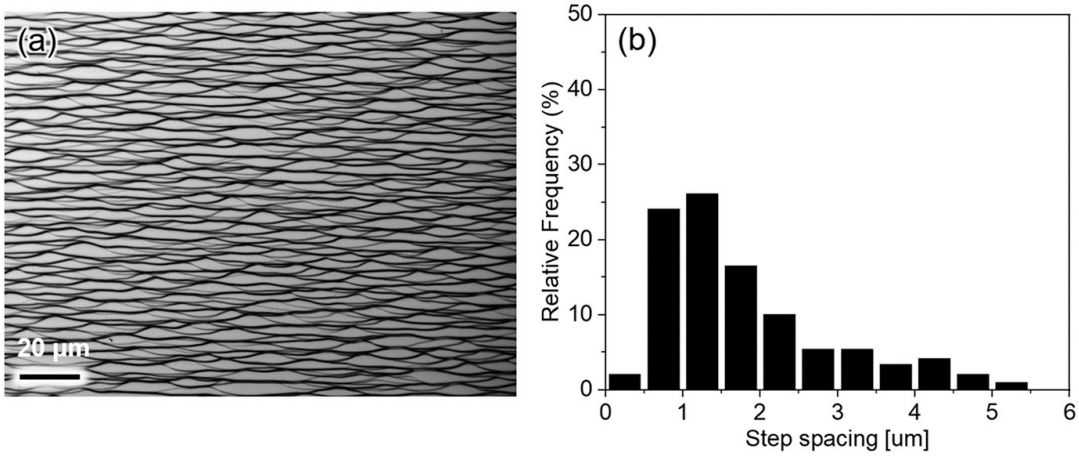

Figure ESM-5 a) surface morphology observed by NDIC optical microscopy of 4H-SiC, 4°off Si-face surfaces treated at 1600 °C after 5 min. The picture was captured in the centre area. At the right b) is displayed the corresponding distribution of step spacing.

ESM-6. Comparison of surface morphologies, shielding the EMF by two different methods

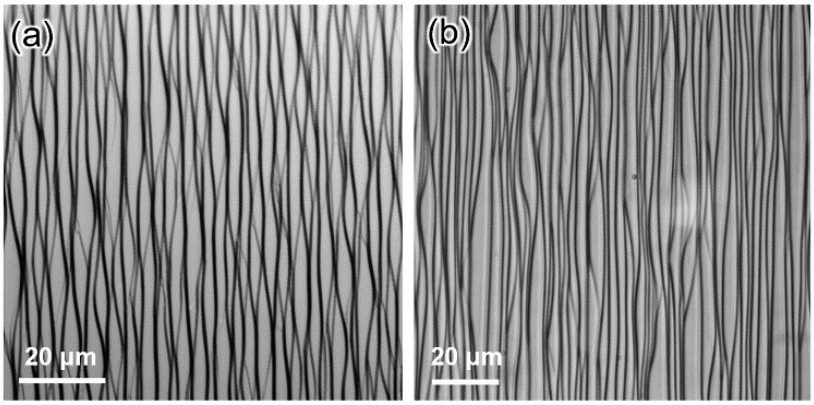

Figure ESM-6 Surface morphology observed by NDIC optical microscopy of 4H-SiC, 4°off Si-face surfaces treated at 1600 °C after 30 min. a) experiment carried out with Ta tube at 22 kHz and b) without Ta tube at 280 kHz. All other conditions being identical.

[1] Scace RI, Slack GA (1959) Solubility of Carbon in Silicon and Germanium. J Chem Phys 30:1551–1555. https://doi.org/doi:http://dx.doi.org/10.1063/1.1730236